AD-A102 140 NAVAL RESEARCH LAB WASHINGTON DC F/G 9/5
ON THE EQUIVALENCE OF TWO-DIMENSIONAL AND THREE-DIMENSIONAL MUL--ETC(U)
JUL 81 J P SHELTON
UNCLASSIFIED NRL-8493 NL

1 OF 1
AD A
102140

END
DATE
FILMED
8 -81
DTIC

NRL Report 8493

On the Equivalence of Two-Dimensional and Three-Dimensional Multibeam Microwave Lenses

J. P. SHELTON

Electromagnetics Branch
Radar Division

July 17, 1981

DTIC
S ELECTE D
JUL 29 1981

D

NAVAL RESEARCH LABORATORY
Washington, D.C.

81 7 28 039

REPORT DOCUMENTATION PAGE		READ INSTRUCTIONS BEFORE COMPLETING FORM
1. REPORT NUMBER NRL Report 8493	2. GOVT ACCESSION NO. AD-A10214 0	3. RECIPIENT'S CATALOG NUMBER
4. TITLE (and Subtitle) ON THE EQUIVALENCE OF TWO-DIMENSIONAL AND THREE-DIMENSIONAL MULTIBEAM MICROWAVE LENSES		5. TYPE OF REPORT & PERIOD COVERED Interim report on a continuing NRL problem
		6. PERFORMING ORG. REPORT NUMBER
7. AUTHOR(s) J. P. Shelton		8. CONTRACT OR GRANT NUMBER(s)
9. PERFORMING ORGANIZATION NAME AND ADDRESS Naval Research Laboratory Washington, DC 20375		10. PROGRAM ELEMENT, PROJECT, TASK AREA & WORK UNIT NUMBERS 61153N; RR 021 05 41; NRL Problem 53-0624-0.
11. CONTROLLING OFFICE NAME AND ADDRESS Office of Naval Research Arlington, VA 22217		12. REPORT DATE 7 July 1981
		13. NUMBER OF PAGES 21
14. MONITORING AGENCY NAME & ADDRESS(if different from Controlling Office)		15. SECURITY CLASS. (of this report) UNCLASSIFIED
		15a. DECLASSIFICATION/DOWNGRADING SCHEDULE

16. DISTRIBUTION STATEMENT (of this Report)

Approved for public release; distribution unlimited.

17. DISTRIBUTION STATEMENT (of the abstract entered in Block 20, if different from Report)

18. SUPPLEMENTARY NOTES

19. KEY WORDS (Continue on reverse side if necessary and identify by block number)

Linear antenna arrays
Planar antenna arrays
Multiple beams
Microwave lenses

20. ABSTRACT (Continue on reverse side if necessary and identify by block number)

This report analyzes the theoretical characteristics of lens-fed multibeam arrays. It is shown that, under proper conditions, it is possible to achieve identical performance from two-dimensional (2D) and three-dimensional (3D) lenses with the same number of ports. The proof of this equivalence requires several steps. It is first noted that lenses and multibeam networks can be equivalent in their performance. Then it is shown that multibeam planar arrays can use exactly the same excitations as linear arrays with the same number of elements. This relationship is treated in detail in an appendix. It is then shown that 2D lenses can feed both linear and planar arrays and that 3D lenses can feed

(Continues)

DD FORM 1473 EDITION OF 1 NOV 65 IS OBSOLETE
1 JAN 73
S/N 0102-014-6601

i

20. Abstract (Continued)

both linear and planar arrays. Thus the desired equivalence between 2D and 3D lenses is established. It is shown that this relationship applies to 3D lenses with square and hexagonal planar arrays. The location of the feed array relative to the lens array required to achieve the 2D-3D equivalence is discussed. An experimental demonstration in which a 37-element linear array is fed by a 3D bootlace lens is described. Finally, it is pointed out that the equivalence relationship holds at only one frequency, because the path lengths through the 2D and 3D lenses are different.

CONTENTS

ON THE EQUIVALENCE OF TWO-DIMENSIONAL AND
THREE-DIMENSIONAL MULTIBEAM MICROWAVE LENSES

INTRODUCTION

Microwave lenses, as well as optical lenses, are designed and analyzed by means of geometrical optics. Their focusing properties are determined by optical path length without regard to wavelength or electrical phase. In this report we consider a class of lens-fed multibeam arrays designed with geometrical optics. We show that these lens-array systems can be equivalent to network-fed multibeam arrays, which are specified strictly in terms of their electrical phase properties. Throughout this report equivalent is taken to mean "having the same scattering matrix," particularly with regard to the transfer coefficients of a matched $2N$-port device. This relationship can be referred to as a lens-network equivalence. Then we recall a property of multibeam arrays which makes certain network-fed multibeam linear and planar arrays equivalent. This relationship is a linear array - planar array equivalence. These two relationships can be applied to show the equivalence of two-dimensional and three-dimensional lenses. The principal practical result of this final equivalence relationship is that, under appropriate conditions a three-dimensional lens can be used to feed a linear array or a two-dimensional lens can be used to feed a planar array. For the former case it will be seen that the maximum dimensions of the lens structure are reduced greatly from the conventional arrangement, in which a two-dimensional lens is used to feed a linear array.

The background of the problem is described and descriptions of microwave lenses and networks are given in the next section. The third section is devoted to the definition of lens-network equivalence. The fourth section discusses the constraints on multibeam arrays. The fifth section applies the array constraints to lenses to arrive at the final equivalence relationship. In the sixth section, a practical example is presented, with a discussion of the limitations of the concept.

BACKGROUND

The class of microwave lenses being considered in this report is exemplified by the bootlace configuration (also known as the Gent or Rotman lens) shown in Fig. 1 [1,2]. This antenna system contains three arrays. One array forms the aperture of the system; another is connected to the feed ports; and the third, the lens array, is internal. The lens and feed arrays face each other across an open, geometrical optical-transmission region. The lens and aperture arrays are connected by transmission lines. Thus, the overall system contains two transmission regions, one unconstrained and one constrained. The lens structure consists of the feed and lens arrays and their enclosed transmission region. The size of the lens is the size of this region. Each feed port corresponds to a directive radiation pattern from the array. The object of the lens design is to make the collimation as good as possible for all beam positions.

In a two-dimensional (2D) configuration, all the arrays are linear, either curved or straight, and the transmission region is generally planar. In order to achieve improved performance, Wild has used a spherical geodesic transmission region [3]. The 2D bootlace lens generates multiple beams in a plane including the aperture array.
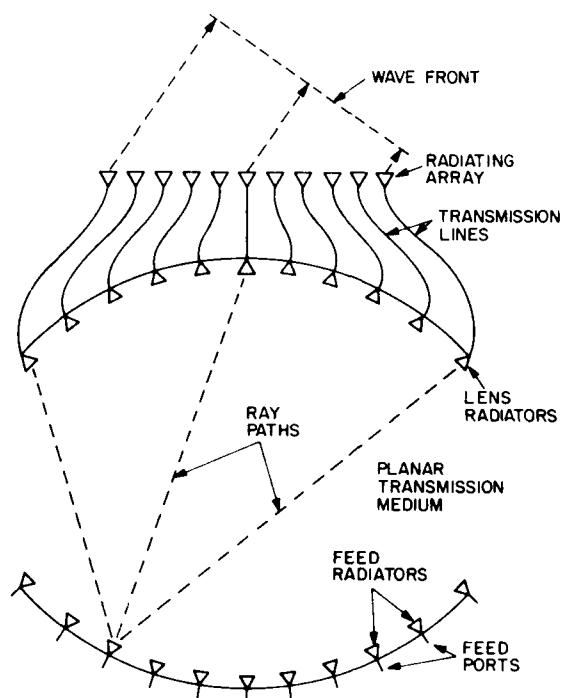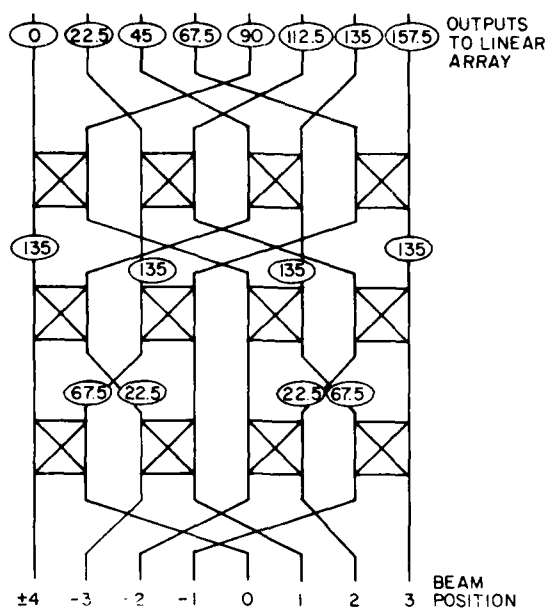
1

Fig. 1 — Gent/Rotman bootlace lens (2D)

In a three-dimensional (3D) configuration, all the arrays are distributed on surfaces, and the transmission region is a volume. The 3D bootlace lens generates multiple beams in two angular dimensions. The locations of the beams in sine space correspond to the locations of the elements in the feed array.

We have seen that these lenses are designed on the basis of geometrical optics. However, the spacings and locations of the radiators in the various arrays are determined on the basis of their diffraction characteristics, and of course the radiation patterns of the multiple beams involve the phases of the elements in the aperture array and the computation of, at the least, a scalar diffraction integral. Thus, although the geometry of the lens, in terms of the surfaces and transmission line lengths, is determined by geometrical optics, the performance is computed by means of physical optics.

It is also necessary to define the networks we are discussing. The most widely known multi-beam network is the Butler matrix, which is shown in Fig. 2 for $N = 8$ [4,5]. Other network configurations can be used, such as those of Blass and Nolen [6,7]. All of these networks approach ideal performance, defined by matched input impedance at all ports for the case in which all ports are properly terminated, perfect isolation among all ports on each side of the network, uniform power division between an input and all output ports, no loss of energy, and uniform phase progression among the output ports for any input port. When one of these networks is connected to a linear array, a perfect multibeam antenna system results: A set of antenna patterns with maximum gain and minimum angular spacing between adjacent beams is obtained.

Fig. 2 — Butler-matrix network for $N = 8$

NETWORK-LENS EQUIVALENCE

The arrays used in the bootlace lens of Fig. 1 must be designed so that each element has a pattern with appropriate coverage and gain. Thus each element of the feed and lens arrays must be designed so that its coverage is limited to the array it is facing. In addition, each array must be designed so that it absorbs without reflection any energy incident upon it from the opposite array. The aperture array must radiate without reflection all energy fed to it by the lens array. The element spacings, using the above criteria, are given by

$$s = \frac{\lambda}{\sin \theta_1 - \sin \theta_2},$$

(1)

where λ is the wavelength and θ_1 and θ_2 are the limits of coverage relative to the normal to the array at the element [8]. In general, θ_1 is positive and θ_2 is negative. A practical lens will not meet these requirements perfectly. Real radiators invariably exhibit some impedance mismatch, mutual coupling, and pattern degradation. However, the departure from perfection can be sufficiently small that these lenses are attractive in many applications.

This author has pointed out that a lens with its arrays designed according to Eq. (1) exhibits performance equivalent to that of a multibeam network with the same number of ports [9]. That is, the transfer coefficients of the lens and the network are identical within the tolerance set by the collimating imperfections inherent in the lens. No proof was given for this claim; numerous computations and measurements have borne out the network behavior of appropriately designed lenses.

3

MULTIBEAM PLANAR ARRAYS

This author has discussed the formation of multiple beams from planar arrays [10]. It was shown that a planar array can be fed by an ideal multibeam network to form multiple beams if the array satisfies a "tiling" condition. The tiling condition requires that the array can cover the infinite lattice of element positions, with no gaps or overlap, by translation of the array, as shown in Fig. 2. It was shown that, in some cases, the planar array can be fed by a linear-array feed network. In particular, all regular hexagonal arrays with a triangular-element lattice and all square arrays with a square-element lattice fall in this category. Thus, the same phase distributions can be used for these planar arrays to form multiple beams as are used for a linear array with the same number of elements. This linear-planar array equivalence is discussed in the appendix.

2D-3D LENS EQUIVALENCE

We are now at the point of establishing the equivalence relationship that is the subject of this report, the equivalence of 2D and 3D lenses. Figure 3 shows the various networks, lenses and arrays and their relationships. It is now possible to apply a syllogistic argument that things equivalent to the same thing are equivalent to each other.

From the standpoint of the phase distributions required to form multiple beams, we have seen that linear and planar arrays are equivalent. Thus, the same network can feed either array. In addition, a multibeam network is equivalent to a 2D lens. Therefore, we conclude that a 2D lens can feed either a linear or a planar array and that, since a 3D lens can feed a planar array, a 3D lens can also feed a linear array. That is, under the proper conditions a 3D lens can have the same network characteristics as a 2D lens. These conclusions are illustrated in Fig. 4.
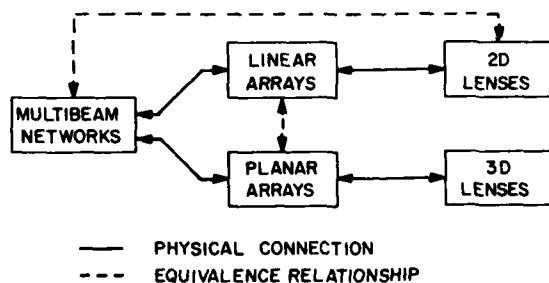

—— PHYSICAL CONNECTION
– – – EQUIVALENCE RELATIONSHIP

Fig. 3 — Network/lens/array relationships

—— PHYSICAL CONNECTION
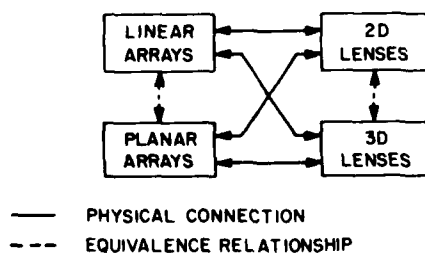– – – EQUIVALENCE RELATIONSHIP

Fig. 4 — 2D-3D lens equivalence

4

We now consider the detailed configuration of a 3D lens that will be equivalent to a given 2D lens. In the appendix the method for feeding a planar array with a linear-array network (or equivalently a 2D lens) is outlined. The final derivation in the appendix indicates the beam locations that will be obtained from the array-network interconnection. We note that the beam location is easily and directly related to the feed location for either a 2D or a 3D lens. Thus, the lattice of beam locations is duplicated by the lattice of feed positions. In the case of the hexagonal array, the beam locations form a hexagonal array which is "twisted" relative to the lens array by an angle $\pi/3 - \phi$, where ϕ is given by Eq. (A12) in the appendix. The size of the feed array is selected so that the path lengths through the lens to the aperture array result in the proper phase distribution at the design frequency. We know the required phase distribution from the derivations of the appendix, and all phases are constrained to be contained within the range 0 to 2π. In determining the required path-length differences, we must take care to avoid the discontinuous phase steps that may be inherent in a modulo 2π phase distribution. Figure 5 illustrates this process for a 19-element hexagonal array. Figure 5(a) is based on Fig. A4(a) in the appendix, except that the integers have not been constrained to modulo 19 and the feed location is indicated. For $N = 19$, the twist angle of the feed array relative to the lens array is 6.59°. Figure 5(b) shows the next feed location out from the center of the lens, together with the corresponding integer aperture distribution. We recall that the element phases are given by the integers times $2\pi/N$. This multiplying factor translates to λ/N for path length. Thus, the path-length differences for the feed locations of Figs. 5(a) and 5(b), relative to elements a and b, are $20\lambda/19$ and $40\lambda/19$, respectively. This information, together with a knowledge of the twist angle and the geometry of the lens, is sufficient to design a 3D lens that is equivalent to a 2D lens.

A PRACTICAL EXAMPLE

In 1975 the Federal Aviation Administration, in carrying out the development of the Microwave Landing System (MLS), investigated the use of microwave optical electronic scanning antenna configurations. The question posed to NRL workers at that time was whether there was any technique available for reducing the size of the microwave optics relative to the array aperture with which it was used. The largest apertures contemplated for MLS were about 3.7m (12 ft) long, and typical 2D bootlace lenses for these apertures will have dimensions larger than this. No alternative
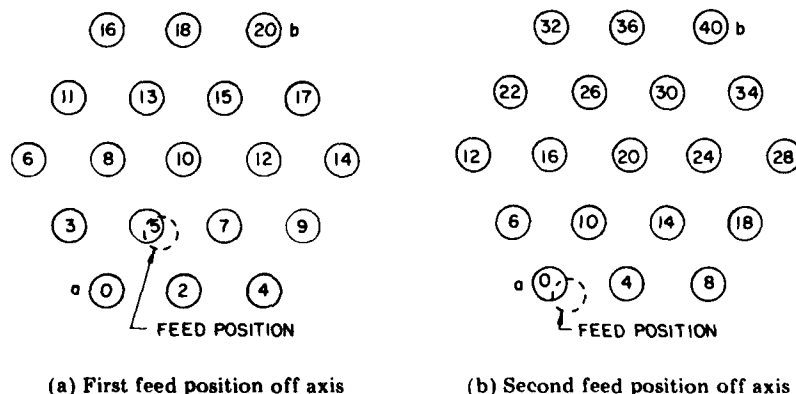
(a) First feed position off axis   (b) Second feed position off axis

Fig. 5 — Integer aperture distributions for 19-element hexagonal array

5

design technique was found in 1975 in spite of intensive effort by workers in both Australia and the U.S.

The equivalence relationship described in this report provides a means for feeding a multibeam linear array with a lens that is much smaller than the array. The degree of this size reduction is roughly estimated by considering that the elements of the feed and lens arrays of the 3D lens will be spaced no more than one wavelength apart. Therefore, the diameter of the 3D lens will be about $\sqrt{N}\lambda$, whereas the aperture of the array will be about $N\lambda/2$ in length. The ratio of lens size to array size is about $2/\sqrt{N}$, and the relative size reduction is seen to increase with N. For $N = 100$ we would expect the lens to be about 1/5 the size of the array.

If the lens is air filled, if we have established the number of elements and the general lens geometry, and if we impose symmetry on the feed and lens arrays, we can determine the lens dimensions. Figure 6 illustrates the geometry of the lens. It is assumed that the arrays are hexagonal. Symmetry dictates that the outer elements of the lens and feed arrays be at the same radius. It can be shown from previously determined relationships that the maximum path length difference for the first feed position off axis is

$$\Delta L_1 = 2r(2r + 1)\lambda/N .$$

For the rth feed position off axis,

$$\Delta L_r = 2r^2(2r + 1)\lambda/N .$$

We find that

$$L_a = \sqrt{S^2 + 4R^2 \sin^2 \gamma/2}$$

and

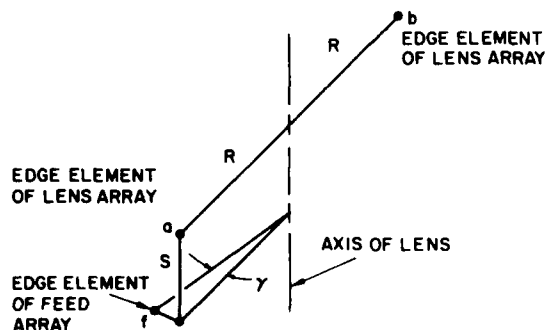$$L_b = \sqrt{S^2 + 4R^2 \cos^2 \gamma/2} ,$$

Fig. 6 — Geometry of edge elements of lens and feed
arrays for symmetrical lens

6

where

S is the spacing between edges of the feed and lens arrays,

R is the radius of the feed and lens arrays,

L_a is the distance between the edge feed element f and edge lens element a,

L_b is the distance between the edge feed element f and edge lens element b,

γ is the twist angle, ϕ $\pi/3$.

Setting $\Delta L_r = L_b - L_a$, we obtain

$$2r^2(2r + 1)\lambda/N = \sqrt{S^2 + 4R^2 \cos^2 \gamma/2} - \sqrt{S^2 + 4R^2 \sin^2 \gamma/2}. \qquad (2)$$

In Eq. (2) the known parameters are r, N, λ, and γ. If S, R, or S/R is specified, the lens dimensions are determined.

This concept has been demonstrated experimentally. An air-filled 3D bootlace lens was fabricated with 37-element hexagonal feed and lens arrays. The array elements are circularly polarized conical spiral radiators. An external view of the lens structure is shown in Fig. 7, and a view of the
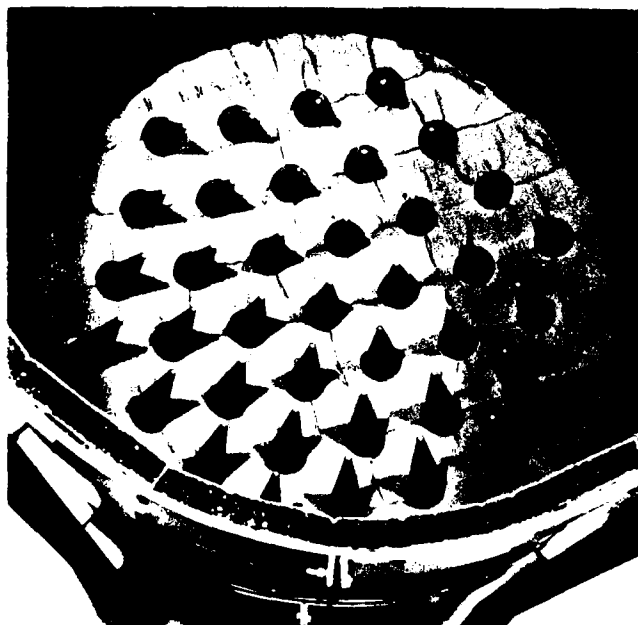

79507(2)

Fig. 7 — Air-filled 3D lens for $N = 37$

7

interior with one of the arrays is shown in Fig. 8. Equal-length coaxial cables are connected between the lens-array ports and a 37-element linear array. The linear array consists of slotted waveguide radiators. The system is designed to operate at 5060 MHz, the center of the MLS band. Figure 9 shows the lens-array assembly being tested on the NRL outdoor pattern range. Figure 10 is a plot of the main beams of the patterns generated by the system. The dashed patterns are grating lobes.
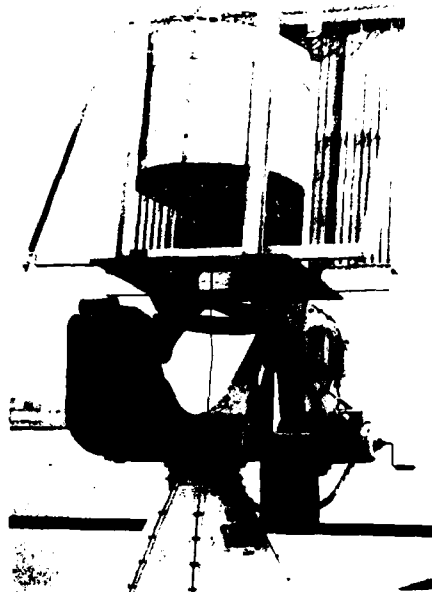
Finally, we note that the equivalence relationships discussed and derived in this report, both between lenses and networks and between 2D and 3D lenses, are valid only at a single frequency. The desired network behavior of the lenses is obtained by transforming path length differences into phase differences. Since the path lengths do not change with frequency, the phase relationships clearly will change with frequency. Furthermore, when 2D and 3D lenses are made equivalent, their phase characteristics will also change with frequency, and they will change differently because the path lengths for equivalent 2D and 3D lenses will be much different. Our original claim of lens-network equivalence was based on appropriate spacing of the radiating elements in the arrays making up the lens. This relationship, Eq. (1), involves wavelength and immediately introduces frequency sensitivity.

These comments on frequency sensitivity should not be confused with other wide-band characteristics of lenses. Since the lenses described here are based on geometrical optics, their beam positions are invariant with frequency. This is sometimes a highly desirable characteristic. Nevertheless, the lens-feed array is still a narrow-band one from the standpoint of its equivalence to an ideal multibeam network, for which the beam positions change with frequency.

79507(3)

Fig. 8 — Lens interior

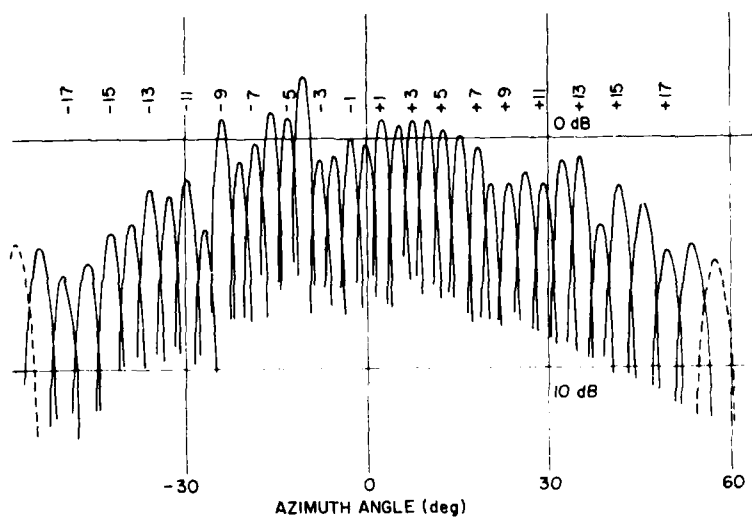79685(1)

Fig. 9 — Lens with 37-element array
on test range

Fig. 10 — Combined plot of all beams from 37-element linear array

ACKNOWLEDGMENT

The valuable assistance of Mr. Allison E. March in design, assembly, and tests of the experimental lens and array is gratefully acknowledged.

REFERENCES

1. H. Gent, "The Bootlace Aerial," Royal Radar Establishment J., pp. 47-57 (Oct. 1957).

2. W. Rotman and R. F. Turner, "Wide-Angle Microwave Lens for Line-Source Applications," IEEE Trans. Antennas Propag. AP-11(6), 623-632 (Nov. 1963).

3. J. P. Wild, "Geodesic Lens," U.S. Patent No. 4114162, Sept. 12, 1978.

4. J. P. Shelton and K. S. Kelleher, "Multiple Beams from Linear Arrays," IRE Trans. Antennas Propag. AP-9, 154-161 (Mar. 1961).

5. J. Butler and R. Lowe, "Beam-Forming Matrix Simplifies Design of Electronically Scanned Antennas," Electronic Design 9, 170-173 (Apr. 12, 1961).

6. W. K. Kahn and E. J. Shubel, "Passive, Series Fed, Multibeam Antenna," *Digest of 1965 International Antenna and Propagation Symposium*, IEEE, New York, Catalog No. 3C12, Aug. 1965, pp. 82-89.

7. J. P. Shelton, "Synthesis of Small Hybrid Multibeam Networks," *Summaries of Papers of International Symposium on Antennas and Propagation*, Institute of Electronics and Communications Engineers, Sendai, Japan, Aug. 1978, pp. 219-222.

8. W. K. Kahn, "Ideal Efficiency of a Radiating Element in an Infinite Array," IEEE Trans. Antennas Propag. AP-15, 534-538 (July 1967).

9. J. P. Shelton, "Focusing Characteristics of Symmetrically Configured Bootlace Lenses," IEEE Trans. Antennas Propag. AP-26, 513-518 (July 1978).

10. J. P. Shelton, "Multibeam Planar Arrays," Proc. IEEE 56, 1818-1821 (Nov. 1968).

APPENDIX

Linear-Planar Array Equivalence

This analysis of planar arrays is based on the following assumptions:

● The feed system is a $2N$-port multibeam network, with N input ports and N output ports which are connected to the array, which becomes a Butler matrix for $N = 2^p$.

● The N-element planar array is located on a regular infinite lattice.

● The array distribution is uniform in amplitude (which follows directly from the use of a Butler-matrix-like feed network) and has linear progressive phases in both dimensions so as to produce a collimated radiation pattern with maximum gain.

This analysis proceeds in several steps. The linear-array feed networks are defined and represented. Then a numbering procedure for the infinite lattice is presented. Then a procedure for defining a specific array is derived. Finally, the beam locations corresponding to a particular array excitation are determined. Results are given in detail for regular symmetrical hexagonal and square arrays.

It is first necessary to define the operation of the feed network. The transfer matrix of the network is defined as

$$E_{ok} = T_{k\ell}E_{i\ell} ,$$

where $E_{i\ell}$ is the ℓth input, E_{ok} is the kth output (feeding the array elements), and $T_{k\ell}$ is the transfer coefficient. We choose, without loss of generality,

$$T_{k\ell} = \frac{1}{\sqrt{N}} e^{j(k-1)(\ell-1)\phi_N} , \quad k = 1, \ldots, N, \quad \ell = 1, \ldots, N , \tag{A1}$$

where $\phi_N = 2\pi/N$. Since the amplitude is constant for all $T_{k\ell}$, it is possible to express the transfer matrix in terms of only the phase. If the exponent is used and the factor ϕ_N is omitted, the matrix portion of $T_{k\ell}$ becomes an array of integers. If we restrict the phase to the range $0 \leqslant \phi < 2\pi$, the term $(k-1)(\ell-1)$ becomes $(k-1)(\ell-1)\mathrm{mod}(N)$, and the highest integer is $N-1$. The resulting integer matrix is defined as $\mathbf{T}_N$, and an example for $N = 5$ is

$$\mathbf{T}_5 = \begin{bmatrix} 0 & 0 & 0 & 0 & 0 \\ 0 & 1 & 2 & 3 & 4 \\ 0 & 2 & 4 & 1 & 3 \\ 0 & 3 & 1 & 4 & 2 \\ 0 & 4 & 3 & 2 & 1 \end{bmatrix} . \tag{A2}$$

Note that every column of $\mathbf{T}_N$ is a linear progressive phase distribution, as is required. Now, since every column provides a progressive phase distribution, it suffices in analyzing arrays fed by

11

this network to use any one that contains all the integers. This is the crucial point on which this analysis depends.

We now consider an infinite square lattice, representing possible radiating element positions. If we are to locate an N-element array on the lattice, the excitation of each element in the lattice can be described by an integer, $n = 0 \ldots N - 1$, where n corresponds to $(1/\sqrt{N})e^{jn\phi_n}$. To satisfy the third assumption, concerning the progressive phase in both lattice dimensions, we are constrained to place integers on the lattice.

Figure A1 illustrates two such lattices for a seven-element array. The shape of a planar seven-element array can be obtained by selecting any seven elements, so long as they include all possible integers. The resulting array can then be fed by a $2N$-port multibeam network to form seven identical patterns, each with maximum pattern gain. Some of the possible array shapes are also shown in Fig. A1. The tiling condition follows directly: Any allowable multibeam planar array can cover the infinite lattice. Completely and without overlap, by translation.

We must next determine how a given planar array will be configured for a multibeam application. Specifically, how will the $2N$-port network be connected to the N-element array? The procedure for determining these connections is as follows.

The given N-element planar array is placed on the lattice with at least two other identical arrays placed around it in a tiling arrangement. Corresponding elements are chosen on three contiguous arrays and are assigned the same integer, say zero for simplicity. This situation is illustrated in Fig. A2 for a seven-element array. We now seek a set of integers for the remaining lattice positions that satisfies the progressive phase requirement. We accomplish this by specifying the integral increment in the two lattice dimensions as n_x and n_y. The equations relating n_x and n_y are

$$n_x X_1 + n_y Y_1 = Np$$

and

$$n_x X_2 + n_y Y_2 = Nq , \qquad (A3)$$

where (X_1, Y_1) and (X_2, Y_2) are components of the vectors R_1 and R_2 defining the translations used to achieve the tiling condition. For the example of Fig. A2, $R_1 = (3, 2)$ and $R_2 = (1, 3)$. The
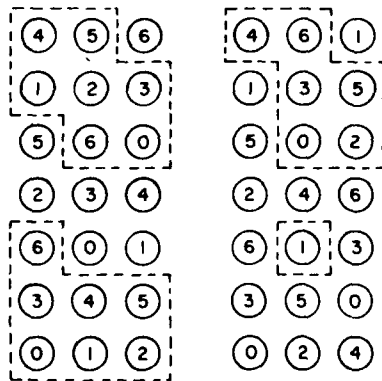

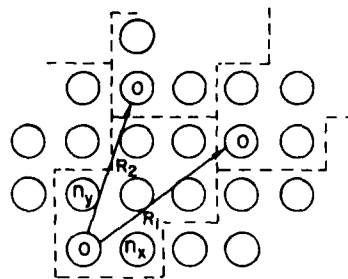Fig. A1 — Lattices for $N = 7$ with possible array shapes

Fig. A2 — Tiling arrangement for seven-element array, showing translation vectors

parameters p and q are integers that determine which of the N possible distributions is obtained; it is usually satisfactory to set $p = q = 1$. Equations (A3) then become

$$3n_x + 2n_y = 7$$

and

$$n_x + 3n_y = 7 \, , \qquad (A4)$$

for which $n_x = 1$ and $n_y = 2$, and the resulting array is shown in Fig. A3(a). Although the array of Fig. A3(a) on its square lattice does not appear particularly interesting, skewing the grid to triangular as indicated in Fig. A3(b) suggests that a seven-element array is the first in a family of regular hexagonal arrays.

The network connection rules for the family of regular hexagonal arrays is readily found if we examine the geometry of the tiling arrangement. If we specify the size of the hexagonal array by r, the number of rings surrounding the center element, then the following results are obtained:

$$N = 3r^2 + 3r + 1 \, ,$$

$$X_1 = 2r + 1 \, ,$$

$$Y_1 = r + 1 \, ,$$

$$X_2 = r \, ,$$

$$Y_2 = 2r + 1 \, ,$$

$$n_x = r \, ,$$

and

$$n_y = r + 1 \, . \qquad (A5)$$

Furthermore, we can take $n_x = mr$ and $n_y = m(r + 1)$, where $m = 1, \ldots, N - 1$, as long as the lattice is still covered by the full range of integers from 0 to $N - 1$. Figure A4 shows interconnection diagrams for 19- and 37-element arrays. If we try all possible values of m, we find six distinct interconnection diagrams for the 37-element array, three for the 19-element array, and one for the
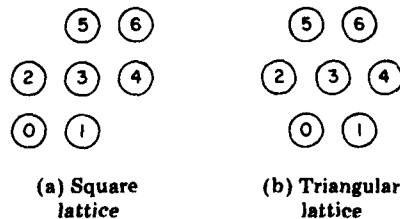

(a) Square   (b) Triangular
    lattice   lattice

Fig. A3 — Seven-element array
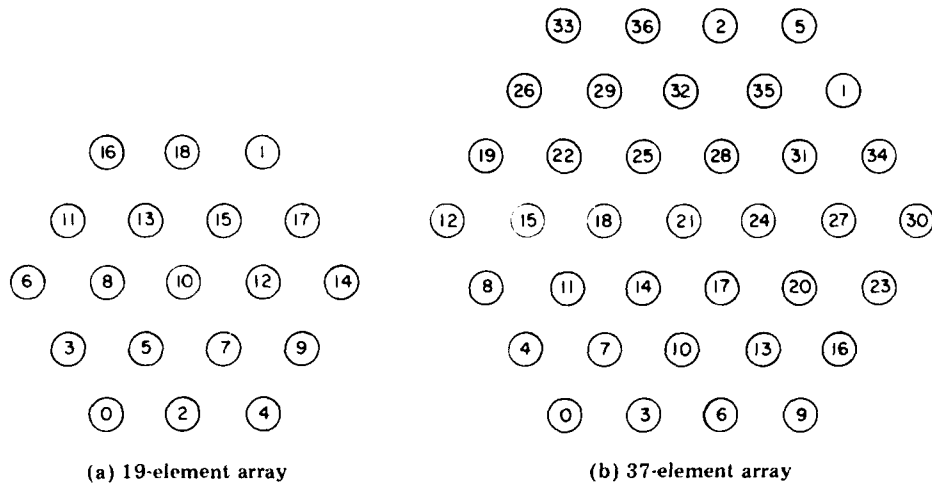
13

(a) 19-element array (b) 37-element array

Fig. A4 — Interconnection diagrams for hexagonal arrays

7-element array. By distinct interconnections we mean that we discard all rotations and mirror images. Allowed values of n_x and n_y are listed in Table A1 for the first four hexagonal arrays. We are led to conjecture that the number of distinct interconnections is $r(r+1)/2$.

Table A1 — Allowed Values of n_x and n_y

N	r	n_x	n_y
7	1	1	1
19	2	2	3
		4	6
		1	7
37	3	3	4
		6	8
		9	12
		2	15
		5	13
		1	10
61	4	4	5
		8	10
		12	15
		16	20
		7	24
		2	26
		11	21
		6	17
		1	13
		3	19

14

A similar analysis can be carried out for square arrays. In this case, it is found that the tiling arrangement is not unique, because the arrays are aligned in strips which can slide relative to one another. However, a tiling arrangement with all possible integers which can be fed by a conventional multibeam network or a 2D lens can also be achieved by offsetting one strip of square arrays by one element relative to the next, as shown in Fig. A5 for $N = 16$. If the square array has r elements on a side, so that $N = r^2$, then the desired tiling arrangement can always be achieved by setting

$$\mathbf{R}_1 = (X_1, Y_1) = (r, 0)$$

and

$$\mathbf{R}_2 = (X_2, Y_2) = (-1, r) .$$

These parameters yield

$$n_x = r$$

and

$$n_y = 1 . \tag{A6}$$

Furthermore, as in the case of the hexagonal array, we can take $n_x = mr$ and $n_y = m$, where $m = 1, \ldots, N - 1$, as long as the lattice is still covered by the full range of integers from 0 to $N - 1$.

We now consider the locations of the beams generated by the hexagonal and square arrays defined by Eqs. (A5) and (A6). If we know the phases of a small triangle of elements in the array, we can locate the beam. The geometry of these triangles is shown in Fig. A6(a). We locate the beams in a Cartesian sine space with coordinates defined as

$$u_x = (2\pi s/\lambda) \sin \theta_x$$
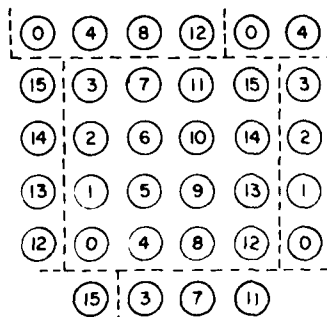
and

$$u_y = (2\pi s/\lambda) \sin \theta_y .$$

Fig. A5 — Tiling arrangement for
square array with $N = 16$

15

We also define radial sine-space coordinates as

$$u_r = \sqrt{u_x^2 + u_y^2} = (2\pi s/\lambda) \sin \theta_r$$

and

$$\tan \phi = u_y/u_x .$$

The geometry of rays approaching the triangular arrays is shown in Fig. A6(b). The equations for the beam location in terms of α and β, which are integers, are

$$\frac{2\pi\beta}{N} = \frac{2\pi s}{\lambda} \sin \theta_r \cos (\pi/3 - \phi) = u_r \cos (\pi/3 - \phi)$$

and

$$\frac{2\pi\alpha}{N} = \frac{2\pi s}{\lambda} \sin \theta_r \cos \phi = u_r \cos \phi \qquad (A8)$$

for the triangular lattice, and

$$\frac{2\pi\beta}{N} = \frac{2\pi s}{\lambda} \sin \theta_r \sin \phi = u_r \sin \phi$$

and

$$\frac{2\pi\alpha}{N} = \frac{2\pi s}{\lambda} \sin \theta_r \cos \phi = u_r \cos \phi \qquad (A9)$$

for the square lattice. Equations (A8) are solved for u_r and ϕ to yield

$$\tan \phi = \frac{(\beta/\alpha) - \cos \pi/3}{\sin \pi/3}$$

and

$$u_r = 2\pi\alpha/N \cos \phi = 2\pi\beta/N \cos (\pi/3 - \phi) \qquad (A10)$$

(a) Geometry of ray   (b) Ray-path projections in plane normal to array
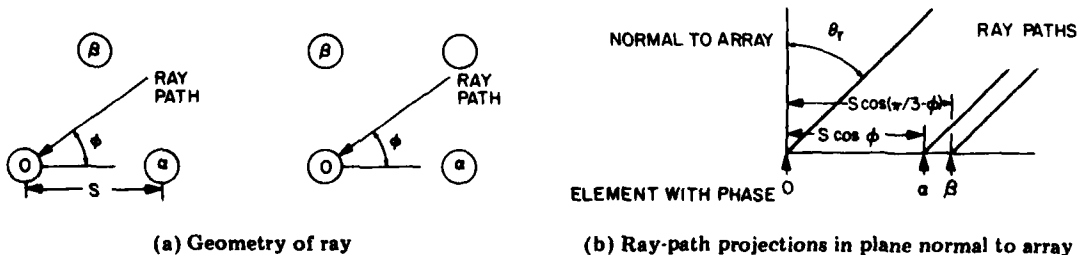
Fig. A6 — Geometry of rays for given array phase distribution

for the triangular lattice. Equations (A9) are solved to yield

$$\tan \phi = \beta/\alpha$$

and

$$u_r = 2\pi\alpha/N \cos \phi = 2\pi\beta/N \sin \phi \tag{A11}$$

for the square lattice.

The nearest grating-lobe maxima for the beam located at $u_x = u_y = 0$ are obtained for the triangular lattice for the following values of α and β:

$$\alpha = \pm N, \ \beta = 0$$

$$\alpha = \beta = \pm N;$$

and

$$\alpha = 0, \ \beta = \pm N.$$

Equations (A10) locate these grating lobes at $u_r = 4\pi/\sqrt{3}$ and $\phi = 0, \pi/3, 2\pi/3, \ldots, 5\pi/3$.

Similarly, the nearest grating lobes for the square lattice are obtained for

$$\alpha = \pm N, \ \beta = 0$$

and

$$\alpha = 0, \ \beta = \pm N.$$

Equations (A11) locate these grating lobes at $u_r = 2\pi$ and $\phi = 0, \pi/2, \pi, 3\pi/2$.

Using Eqs. (A5) and (A6) to define α and β, we obtain the following beam locations:

$$\alpha = r,$$

$$\beta = 2r + 1,$$

$$u_r = 2\pi/\left(\sqrt{N} \sin \pi/3\right),$$

and

$$\cos \phi = (r \sin \pi/3)/\sqrt{N} \tag{A12}$$

for the triangular lattice and

$$\alpha = r,$$

$$\beta = 1,$$

$$\tan \phi = 1/r,$$

and

$$u_r = 2\pi\sqrt{N+1}/N \tag{A13}$$

17

for the square lattice. These results are illustrated in Fig. A7 for a 19-element hexagonal array and a 16-element square array. The beams are numbered according to how far off the axis of the 2D lens the feed port corresponding to the given beam is located. It is seen from Eqs. (A10) and (A11) that if we move away from the axis of the 2D lens we move away from the origin of sine space on a radial line; that is, ϕ stays constant and u_r increases directly with α or β. By doing so, we are able to locate and number all beam positions.

Two features of the beam locations shown in Fig. A7 are noteworthy. For the hexagonal array, the lattice of the beam locations is rotated relative to that of the array. The "twist" angle is $\gamma = \phi - \pi/3$, for which we find $\sin \gamma = 1/2\sqrt{N}$. The twist relationship will be important in arranging the feed and lens arrays of 3D lenses for use with linear arrays. Furthermore, the integer arrangement for beam locations corresponds to one of the arrangements shown in Table A1 for element assignments. For the square array, the lattice of the beam locations is distorted, with the horizontal rows of beams being tilted up by an angle ϕ. The dashed lines separate cells of grating lobes. Thus, in a practical application we would probably desire to locate the visible region within the central cell. Note that for the hexagonal array it would be possible to locate the circular visible region so as to include only one maximum of all 19 beams. For the square array, however, beams ± 2, ± 6, and ± 8 have two maxima equidistant from the origin. It is not possible to obtain single maxima for these beams without translating all beam locations relative to the origin.

(a) 19-element hexagonal array   (b) 16-element square array
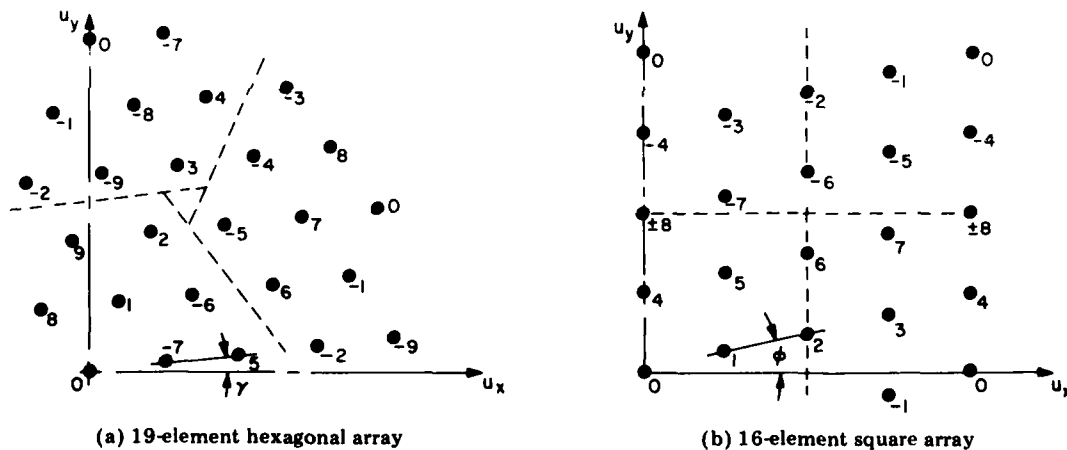
Fig. A7 — Beam locations in sine space for square and hexagonal arrays